Chapter 3

Material and Methods

3.1 Instruments Used in Experimentation

Table 3.1 contains a detailed list of the instruments that have been used throughout the course of the experimental work in this study.

Table 3.1: Instruments used in experimental work

Instruments	**Model**	**Uses**
Electronic analytical balance	CG 103L, India	Measure the mass of chemicals
pH meter	EC PH TUTOR S, India	Measure activity of hydrogen ions in solution
Muffle furnace	NSW-103, India	For sample drying
Scanning Electron Microscope (SEM)	RA-ZEI-005, UK ZEISS MA15/18 make, Germany	Analyzing material's surface
Fourier transform Infrared spectrophotometer (FTIR)	NICOLET spectrophotometer (iS5), USA	To identify organic, inorganic and polymeric materials
X-ray diffraction (XRD)	Rigaku SmartLab 9kW Powder type/Tokyo, Japan	To ascertain a material's crystallographic structure
Thermogravimetric analysis (TGA)	Shimadzu TGA-50 H, Japan	To determine the thermal stability of a material
Atomic Absorption Spectrophotometer (AAS)	PinAAcle 900 Perkin Elmer, USA	To determine the concentration of a particular element in a sample

Shaking Incubator	CIS-18 PLUS, India	To provide aeration To evenly distribute powder sample in solution
Centrifuge	REMI C-24PLUS, India	Separation of fluids on the basis of density
Refrigerator	0ABWRR19N2112UZ, India	To preserve sample

3.2 Characteristic Analysis of Novel Adsorbents

3.2.1 Proximate and Ultimate Analysis

In order to assess the amount of moisture, volatile matter, ash content, and fixed carbon in novel adsorbents, this analysis was carried out [183]. The proximate analysis was carried out using gravimetric methods, and the moisture content was estimated by weight difference after heating the sample at 105ºC for 2 hours in a furnace. The amount of ash produced was calculated by heating the sample in a muffle furnace at 550ºC for 2 hours until no mass variation was observed [183]. The standard procedure was used to acquire the volatile matter [184], and the fixed carbon was calculated by subtracting the percentages of moisture, volatile matter, and ash from the sample. The higher the concentration of fixed carbon, the greater the adsorption capacity of the resulting sample [185]–[187]. The ultimate analysis determined the proportions of C, H, N, S, and O in the sample. The elements C, H, N, and S were determined using a CHN 1000 Leco and a FISONS EA1108 elemental analyzer, and the oxygen percentage was calculated using the difference.

3.2.2 Yield (%)

In order to compute the yield of producing material 'b' from precursor material 'a', Eq. 3.1 were used [188].

$$Yield(\%) = \frac{W_b}{W_a} \times 100 \tag{3.1}$$

where, W_b is weight of producing material (g) and W_a is weight of precursor (g).

3.2.3 Bulk Density

The bulk density (kg/m^3 or g/cm^3) of a sample is denoted as its weight per unit volume of the measuring cylinder. It is largely employed in the production of amorphous materials [186]–[189]. When performing a bulk density test, the flow consistency and package volume of the solid sample are typically calculated. It has been determined in accordance with ASTM method D7481-18 [190]. Eq. 3.2 depicts the correlation that was used to calculate the bulk density of the sample.

$$D_B = \frac{(M_2 - M_1)}{V} \tag{3.2}$$

where, M_2 is mass of measuring cylinder and sample (g), M_1 is mass of measuring cylinder (g), D_B is bulk density (g/cm^3) and V is volume (cm^3).

3.2.4 Iodine Number

Small compounds like iodine, for example, are primarily adsorbed on carbon. It is a measurement of the activity level of the carbonised material (a higher value indicates a higher activation level), and it is generally represented in mg/g [191]. The iodine number can be determined using standard method ASTM D4607-14 (2021) [192].

3.2.5 Brunauer-Emmett-Teller Surface Area

The BET technique was used to calculate the specific surface area of the adsorbents. The BET analyzer was utilised to determine the surface area (Nova 3200e, Quntachrome instruments make, USA). Nitrogen adsorption in the capillary condensation zone is proportional to the pore volume (V_p) [185]–[189].

3.2.6 pH_{ZPC}

The pH value at which the adsorbent surface becomes totally neutral, with both positive and negative surface functionalities, is known as the zero-point charge. The surface is positively charged below this value and negatively charged above it. When it comes to

bonding, cations and anions prefer negatively and positively charged surfaces, respectively [193]. In the present study, deionized water was mixed with a specific amount of novel adsorbent in 100 mL conical flasks. The pH of these flasks was kept between 2 and 12 by using 0.1 M HCl and 0.1 M NaOH. The solutions were agitated at a speed of 100 rpm for 24 hours at 25 °C. After the defined time, the pH of the solution was measured again [194].

3.2.7 Surface Characteristics

SEM was used to determine the topography of the novel adsorbents. The micrograph revealed the structure of pores. EDX analysis was used in this study to determine the elementary composition of the ATA, AC, composite, and mould [185]. The functional groups present on the surface of ATA, AC, composite, and mould were determined using FTIR spectroscopy. The present work utilized FTIR with a wavenumber range of 400 - 4000 cm^{-1} [187].

3.2.8 Crystallinity and Thermostabilization Characteristics

XRD was used to determine the crystallinity of ATA, AC, composite and mould. These adsorbents were analyzed in a diffractometer at 40 kV/15 mA with scanning rate of 2θ per second [195].

In XRD, FWHM (Full Width at Half Maxima) has been used to measure the crystal size of the ATA by using the Scherrer equation [196]:

$$FWHM\ (2\theta) = \frac{K\,\lambda}{L\,cos\theta} \tag{3.3}$$

where, K is a dimensionless form factor close to unity. The form factor has a standard value of approximately 0.9, but this differs with crystallite shape. L is line broadening at half of the full intensity (FWHM) after the instrumental line has been subtracted, in radians. It is referred to as 2θ. Here, θ is Bragg's angle and λ is X-ray wavelength.

Thermogravimetric analysis (TGA) of ATA, AC, composites, and mould was carried out

in a thermogravimetric analyzer using a nitrogen flow rate of 100 ml/min and a heating rate of 10 °C/min up to 1000 °C. TGA was used to evaluate the novel adsorbents' thermal stability [187].

3.3 Experimental Procedure for Adsorption Study

The experimental procedure for adsorption of Cu^{2+}, Ni^{2+} and Zn^{2+} ions on novel adsorbents have been described below.

3.3.1 Standards and Reagents Preparation

The reagents utilized in this study were all analytical grade, and they were not altered in any way. Diluting samples and preparing necessary solutions are done using deionized water (Milli-Q Millipore), while cleaning different types of adsorbents is done with double distilled water. Deionized and double distilled water differ in terms of purity and cost.

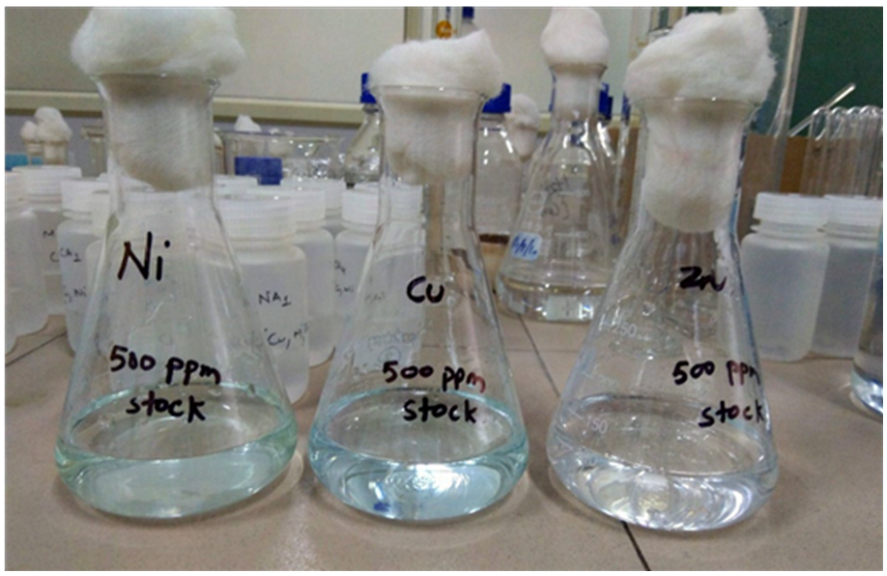

Figure 3.1: Stock solution of Ni^{2+}, $Cu^{2+}$and Zn^{2+} ions

When compared to double distilled water, deionized water is more expensive. As a result, if the user demands a big volume of water for cleaning various adsorbents, double distilled water is needed. Stock solution of 500 mg/L of Cu^{2+}, Ni^{2+} and Zn^{2+} ions (Figure 3.1) was prepared by adding 0.13 g of copper chloride ($CuCl_2.2H_2O$), 0.2025 g of nickel chloride

($NiCl_2.6H_2O$) and 0.104 g of zinc chloride ($ZnCl_2$) salts in 0.1 L of deionized water in labeled conical flasks. The working solutions of variable concentration were prepared by diluting the stock solution with deionized water. The pH of the solution was regulated with either 0.01 M HCl or NaOH.

3.3.2 Selection of Adsorbents for Preparing Novel Adsorbents

Researchers have experimented with a variety of adsorbents to remove Cu, Ni and Zn from solution. Activated carbon is a type of adsorbent that is commonly used in most papers [197], [198]. Some researchers have made it with the help of biomass [199]–[202] and others used commercially available activated carbon [203], [204]. Because of its porous texture and large surface area, activated carbon has a high adsorption capacity [199]. Another advantage of utilizing activated carbon is its chemical nature, which makes surface modification with chemical pre-treatment easier [205]. In this study, we used novel adsorbents and examined their adsorption capacity as well as their efficacy at removing contaminants.

Raw adsorbents that are used in this work was bentonite clay, red ochre, *Tectona grandis* sawdust, *Azadirachta indica* twigs and Natural soil for preparing various novel adsorbents. Effect of various parameters was checked using these adsorbents and a comparative analysis of their adsorption capacity has been done. The reusability test of each adsorbent has been also done to elucidate which adsorbent can be reused. The preparation of novel adsorbents from their raw materials is mentioned below.

3.3.2.1 Composite of Bentonite Clay and Red Ochre

Composite material was prepared by adding an equal amount of red ochre and bentonite clay in a ratio of 1:1. The blending was done uniformly till the attainment of granulation in an automatic grinder-cum-mixer. The blend was supplied in pellet manufacturing machine (GEMCO Energy Machinery Co., Ltd make, China) and pellets (composite material) were harvested out of sampling port (Figure 3.2).

Figure 3.2: Composite beads made from bentonite clay and red ochre

3.3.2.2 *Azadirachta indica* Twig Ash (ATA)

The ATA was collected from mud chula from Chitupur, a village in Varanasi, Uttar Pradesh, India. While collecting the ATA from mud chula, it was observed that approximately 30 minutes are required to convert *Azadirachta indica* twig into ash after ignition.

(a) Dried neem twigs used in mud stove

(b) Ash after food preparation

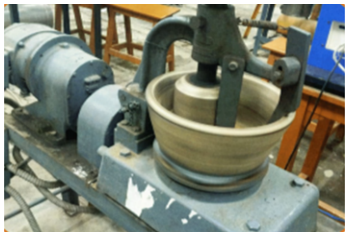

(c) Particle refining by edge runner machine

(d) Separation of particles in different mesh sizes by gyratory sieve shaker

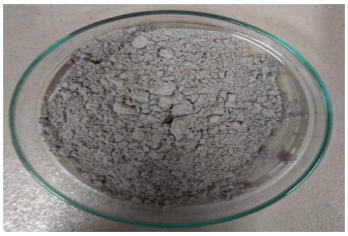

(e) Product in its final form (*Azadirachta indica* twig ash powder)

Figure 3.3: Process of preparation of ATA

The collected ash was washed thrice with doubled distilled water and dried at 105 °C till its weight became constant in a hot air oven (KBR Industries make, India). The dried ash

powder was sieved for less than 145 μm in a gyratory sieve shaker (Khera Instruments Pvt. Ltd. make, India). The residual obtained was packed in polyethylene airtight bags for conducting batch experiments. The process was shown in Figure 3.3 Afterward, the prepared material was characterized and used to adsorb ternary metal ions from liquid phase.

3.3.2.3 Activated Carbon derived from *Tectona grandis*

Tectona grandis sawdust (TG) (Figure 3.4) was gathered from a local sawmill near the campus of the IIT (BHU) Varanasi.

Figure 3.4: *Tectona grandis* sawdust

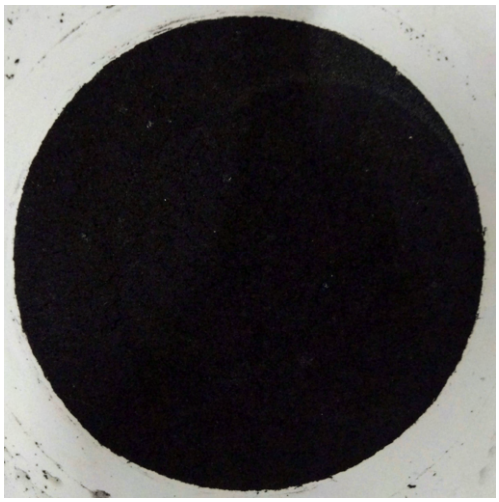

Figure 3.5: Activated carbon derived from *Tectona grandis* sawdust

The TG from a local sawmill was sieved to separate particle sizes. After sieving, it was

rinsed three times with double distilled water and dried for an hour at 105 °C [183].

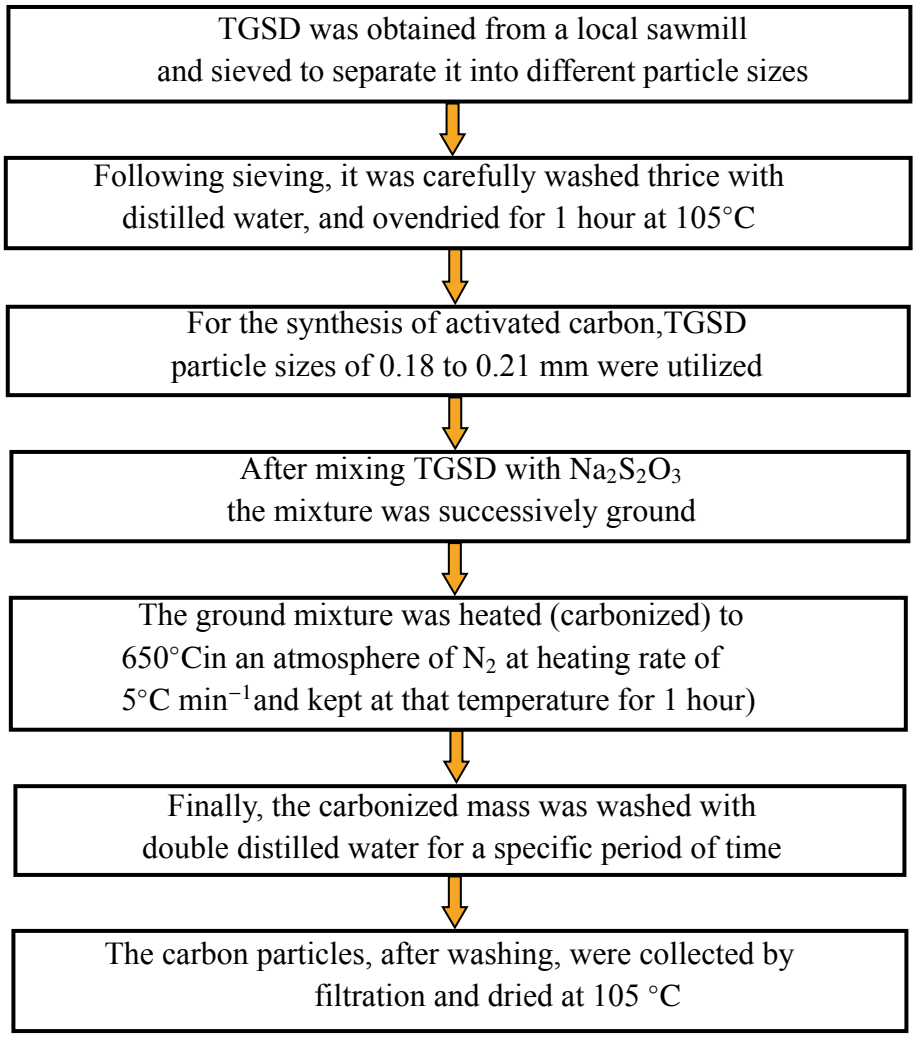

Figure 3.6: Process for producing activated carbon from *Tectona grandis* sawdust

In order to prepare activated carbon, TG was utilized in this study, with a particle size of 80 mesh. The mixture of 20 g TG, 30 g KCl, and 20 g $Na_2S_2O_3$ was successively ground. The whole process of formation of activated carbon is shown in Figure 3.6. As a result, AC have been produced from TG and shown in Figure 3.5.

3.3.2.4 Mould

The bentonite clay and the soil were mixed in equal proportion to make a mould (Figure 3.7a). The mould was then sun dried and placed in a muffle furnace at a temperature of 380ºC for 2 hours and cooled to room temperature (Figure 3.7b). Thereafter, it was used as an adsorbent in experiments.

(a) **(b)**

Figure 3.7: (a) Mould preparation by the potter and (b) Final Product (Mould)

3.4 Batch Adsorption Study

The percentage removal of Cu^{2+}, Ni^{2+} and Zn^{2+} ions as well as the adsorption capacity of each adsorbent, were calculated by Eq. 3.4 and Eq. 3.5.

$$\% \; Removal = \frac{C_i - C_e}{C_i} \times 100 \tag{3.4}$$

$$q = \frac{(C_i - C_e) \times V}{m} \tag{3.5}$$

where, C_i, C_e, V and m are initial and equilibrium concentration (mg/L), volume of solution (L) and mass of adsorbent (g).

These statistical error functions, such as SSE and χ^2 test were used to validate the best fit, appropriateness, and agreement of kinetic and isotherm models. In Eq. 3.6 and Eq. 3.7, the mathematical expressions for SSE and χ^2 are shown.

$$SSE = \sum_{i=1}^{n} \left(q_{e,\,cal} - q_{e,\,exp}\right)^2 \tag{3.6}$$

$$\chi^2 = \sum_{i=1}^{n} \frac{\left(q_{e,\,exp} - q_{e,\;cal}\right)^2}{q_{e,\,cal}} \tag{3.7}$$

where, $q_{e,\ cal}$ is calculated value of adsorption capacity

$q_{e,\ exp}$ is experimental value of adsorption capacity and n is the number of data points. Better agreement between the experimental and the calculated values of metal ions adsorbed was assessed by these models.

Experiments for process parameter optimization were conducted by adding a predefined amount of adsorbents to a solution of varying concentration (mg/L). The pH, temperature and contact time of the operation were all regulated within a range.

After the experiments were completed, samples were collected from the flask and filtered. Atomic absorption spectroscopy was used to analyze the samples. The wavelength used for the analysis of Cu^{2+}, Ni^{2+} and Zn^{2+} ions are 324.8, 352.1 and 214.1 nm, respectively. A slit of 0.5 nm was employed before the flame only to control the intensity of the incident radiation and current were set to be 5 mA with flame of C_2H_2/Air.

All tests were performed thrice, and the study utilized the average value. The error bars in each figure represent the standard deviations of triplicate experimental data.

3.5 Factors Affecting Adsorption

3.5.1 Contact Time

Before reaching equilibrium, the removal efficiency increases with the contact time [206]. The contact time ranges used in the experimental study were 0-330 minutes, 0-210 minutes, 0-30 minutes, and 0-30 minutes for the composite, ATA, AC, and mould, respectively, with the materials under investigation.

The amount adsorbed at equilibrium represents the adsorbent's maximum adsorption capacity under the operating conditions.

3.5.2 pH

A significant influence in the process of adsorption is played by the pH of the solution [207]. Aside from that, its effect is dependent on the charge on the adsorbent's surface [208]. The pH ranges used in the experiments were 2 to 6, 3 to 11, 8.8 to 10, and 2 to 10

for composite, ATA, AC, and mould, respectively.

3.5.3 Initial Concentration

The adsorption capacity at various metal concentrations was calculated using a fixed amount of adsorbent and a variable initial metal ion concentration.

The range of initial concentration used in the experiments were 10 to 100 mg/L for composite, ATA and AC and 10 to 50 mg/L for mould. The initial and final concentrations of metal ions in the tests were determined using AAS. The adsorption capacity of the adsorbents was determined using existing data.

3.5.4 Adsorbent dose

The adsorbent dose is a crucial parameter since it determines the adsorbent's capacity [206]. The influence of adsorbent dose on the adsorption process was examined in this study by altering the amount of adsorbents used while maintaining all other parameters constant. The amount of adsorbent dose taken in the experimental work were 1-2 g/100 mL for composite and ATA, and 0.1 to 1 g/100 mL for AC.

3.5.5 Temperature

Adsorption capacity rises with temperature, showing that the process is endothermic and is enhanced at higher temperatures. As the temperature rises, the intermolecular forces between adsorbate and adsorbent become significantly stronger than those between adsorbate and solvent [209]. The range of temperature used in the experiments were 288 to 308 K for composite, ATA, AC and mould.

3.6 Adsorption Dynamics

Mass transfer at interfaces is involved in many natural and industrial processes. Adsorption and other interfacial characteristics are important in applications such as wetting and

coating [210]. Surface adsorption mechanistic knowledge frequently presupposes molecular diffusion in the bulk solution and subsequent adsorption at the interface. Fick's law accurately describes diffusion, but adsorption kinetics is rather well recognized [210].

This study utilizes a generalised theoretical model for adsorption dynamics at the air-liquid interface, as well as a new kinetic equation based on SRT. The novel kinetic equation, like many previously published kinetic equations, contains a number of parameters, yet all of these parameters are theoretically attainable [210].

The adsorption dynamics of the process were determined by three dimensionless numbers: ψ (ratio of adsorption thickness to diffusion length), λ (ratio of adsorption thickness squared to the ratio of adsorption to desorption rate constant), and N_k (ratio of the adsorption rate constant to the product of diffusion coefficient and bulk concentration). The suggested model is used to perform and verify numerical simulations for surface adsorption [210]. Metal ion adsorption at the solid-liquid interface occurs in three stages: bulk diffusion, surface (film diffusion), intraparticle diffusion, and reshuffling [211], [212]. The step that determines the rate of adsorption can be any of the steps outlined previously. However, reshuffling is a rather speedy process and so is not frequently regarded a rate-determining phase. Based on the study of Borwankar et al., 1988 [211] film diffusion is dominant if D_f $\left(0.23 \frac{r_0 \partial}{t_{1/2}} \times \frac{\overline{C}}{C}\right)$ ranges from 10^{-6}-10^{-8} cm^2/sec and pore diffusion if D_p $\left(0.03 \frac{r_0^2}{t_{1/2}}\right)$ ranges from 10^{-11} to 10^{-13} cm^2/sec. Here, r_0 is radius of adsorbent (cm), ∂ is film thickness (cm), $t_{1/2}$ is time for half change(sec) and $\frac{\overline{C}}{C}$ is equilibrium loading of adsorbent.

In addition to this, in the present work dimensionless numbers were derived to elucidate the role of mixed diffusion-cum-transfer (film) controlled mechanism during adsorption in the liquid phase. The derivation assumes that Arrhenius rate formulations are of high order and molecularity. The derivation also considers n^{th} power relationship between activation energy and surface concentration of active sites. These models are empirical and by incorporating experimental data the model parameters have been evaluated.

3.6.1 Derivation of Dimensionless Numbers

The spherically symmetrical diffusion of ligands is regulated by Fick's second law of diffusion (Eq. 3.8).

$$\frac{\partial C}{\partial t} = \frac{D}{s^2}\frac{\partial}{\partial s}\left(s^2\frac{\partial C}{\partial s}\right) \tag{3.8}$$

where, D is the diffusion coefficient (m^2/s), C is the bulk concentration (mol/m^3) and s is the spherical radial coordinate (m).

In order to complete the model description, it is necessary to specify the movement of molecules from the subsurface to the surface.

For the i^{th} ligand molecule, the mass balance at the interface (Eq. 3.9) is

$$\frac{dS_i}{dt} = \emptyset_b^i - \emptyset_d^i \tag{3.9}$$

where, S_i is the i^{th} surface concentration of molecule at adsorption and desorption fluxes ϕ_b and ϕ_d. The adsorption flux, in most physical models, depends on surface concentration (S) and subsurface concentrations (C_s) of ligands, whereas the desorption flux is dependent only on 'S' [213].

The control equations have been rewritten concerning dimensionless parameters for simplicity in mathematical interventions and numerical solutions (as shown in Eq. 3.10).

$$C^* = \frac{C}{C_0}, \quad \varsigma = \frac{r}{r_s}, \quad S^* = \frac{S}{S_\infty}, \tau = \frac{tD}{k^2} \tag{3.10}$$

where, C^* is the dimensionless concentration, C is the bulk concentration (mol/m^3), C_0 is the initial bulk concentration (mol/m^3), ς is the dimensionless distance, r is the spherical radial coordinate (m), $r_{s'}$ is the drop radius (m), S^* is the dimensionless surface concentration, S_∞ is the maximum surface concentration (mol/m^2), τ is the dimensionless time and K is the ratio of surface concentration at equilibrium to bulk concentration. Substituting Eq. 3.10 into Eq. 3.8 yields Eq. 3.11:

$$\frac{\partial C^*}{\partial t} = \varphi^2\left[\frac{\partial^2 C^*}{\partial \varsigma^2} + \frac{2}{\varsigma}\frac{C^*}{\partial \varsigma}\right] \tag{3.11}$$

where,$\varphi = \frac{h}{r_s}$ and h is adsorption thickness (m).

$$\frac{dS^*}{d\tau} = N_k \left[\frac{C_s^*}{S^*}(1 - S^*) - \lambda \frac{S^*}{C_s^*} \left(\frac{1}{1 - S^*} \right) \right] \tag{3.12}$$

Incorporating dimensionless parameters from Eq. 3.10, the transfer kinetic equation (Eq. 3.12) and three dimensionless numbers φ, $\lambda$and N_k get summarized in to Eq. 3.13:

$$\varphi = \frac{h}{r_s}, \qquad \lambda = \frac{h^2}{K}, \qquad N_k = \frac{K_a}{DC_0} \tag{3.13}$$

where, K_a is adsorption rate constant (mol/m s)

The lower values of φ and λ signifies maximum surface area coverage of biosorbent by ligands with least surface tension at solid liquid interface [213]. The three different modes (diffusion-controlled, mixed diffusion and transfer controlled, and transfer controlled) primarily depend on the value of N_k. According to Joos and Serrien, 1989 [213] adsorption dynamics is:

i. diffusion controlled for values of N_k 10^1 to 10^4

ii. mixed diffusion and transfer controlled of N_k 10^{-3} to 10^1

iii. transfer controlled for values of $N_k 10^{-4}$ to 10^{-3}

3.7 Mechanistic Modeling

3.7.1 Bangham Model

Bangham model [214] determines the role of film diffusivity during adsorption. The model has been represented in Eq. 3.14.

$$Log \left[\log \left\{ \frac{C_0}{C_0 - q_t m} \right\} \right] = log \left\{ \frac{k_0 m}{2.303\ V} \right\} + \alpha \log t \tag{3.14}$$

where, k_o (L/g) and α (<1) are the Bangham's equation constant [215].

3.7.2 Boyd Model

Boyd's kinetic model was applied to determine influence of film diffusion in the liquid phase [214]. Boyd model has been expressed in Eq. 3.15a.

$$\beta_t = \ln(\frac{\pi^2}{6}) - \ln(1 - F(t)) \tag{3.15a}$$

$$\beta_t = \left(\sqrt{\pi} - \sqrt{\pi - \frac{\pi^2 \, F(t)}{3}} \right) \tag{3.15b}$$

$$F = \frac{q_t}{q_e} \tag{3.15c}$$

where, F is the fractional attainment of equilibrium at time t (min) and β_t is the mathematical function of F.

3.7.3 Mass Transfer Model

Imaga and Abia, 2015 [216] adopted mass transfer model for diffusion system in cylindrical coordinates. The model has been shown in Eq. 3.16a and Eq. 3.16b.

$$C_0 - C_t = D \exp(k_0 t) \tag{3.16a}$$

$$ln\,(C_0 - C_t) = \ln D + k_0 t \tag{3.16b}$$

where, D is the fitting diameter. The mass transfer model is followed when the plot (ln (C_o-C_t) vs t) is linear. Equation parameters (K_o and D) are slope and intercept of the plot.

3.8 Adsorption Kinetics

The study of wastewater adsorption kinetics is significant because it shows the reaction mechanisms. In order to set up an effective sorption treatment plant, it is also necessary to determine the time required to remove the adsorbate from aqueous solution [217]. An adsorption kinetic model, which is commonly used to estimate the adsorption rate, gives

crucial information about the mechanism of the adsorption reaction [218].

Pseudo first order (PFO) , Pseudo second order (PSO), Elovich, and intraparticle diffusion (IPD) model are some of the kinetic models used to explain the mechanism of adsorption of adsorbate from aqueous solution onto an adsorbent.

3.8.1 PFO Kinetic Model

PFO model implies that ligands attach to solid surfaces in a reversible manner, and that the rate of adsorption is dependent on the number of unoccupied active sites [219]. Non-linearized form of PFO has been shown in Eq. 3.17.

$$\frac{dq_t}{dt} = k_1 (q_e - q_t) \tag{3.17}$$

where, k_1 (min^{-1}) is the rate constant of the pseudo-first-order adsorption reaction. On integration at boundary conditions as $q = 0$ at t = 0 and $q = q_e$ at t = t, Eq. 3.17 reduces to Eq. 3.18.

$$ln (q_e - q_t) = -k_1 t + \ln q_e \tag{3.18}$$

3.8.2 PSO Kinetic Model

PSO kinetic expression was proposed by Ho and McKay to represent the adsorption of metal ions onto the surface of an adsorbent material [220] and it assumes the chemisorption mechanism of ligand binding [219]. The rate expression has been represented in Eq. 3.19.

$$\frac{dq_t}{dt} = k_2 (q_e - q_t)^2 \tag{3.19}$$

where, k_2 (g/mg/min) is the PSO rate constant. The integrated second-order rate equation at boundary conditions q = 0 at t = 0 and q = q_e at t = t has been shown in Eq. 3.20.

$$\frac{t}{q_t} = \frac{1}{k_2 q_e^2} + \frac{1}{q_e} t \tag{3.20}$$

3.8.3 Elovich Model

The Elovich kinetic model concept is based on chemisorption phenomena, which are described further below using Eq. 3.21 [221].

$$q_t = \frac{1}{\beta} ln\,(\alpha\beta) + \frac{1}{\beta} \ln t \tag{3.21}$$

where, α is the initial adsorption rate (mmol/ (g min)) and β is the desorption constant (g/mmol).

3.8.4 IPD Model

The Weber-Morris IPD model is used to deduce the mechanism behind the adsorption process. Adsorption is governed in the aqueous process by bulk diffusion, surface (film diffusion), IPD, and reshuffling [216]. The diffusion can be controlled individually or in combination (mixed diffusion) by either of the steps described above.
However, the reshuffling of ions in cylindrical coordinates on the solid surface is very quick and so, it is not a rate determination step [215]. IPD model is expressed in Eq. 3.22.

$$q_t = k_p t^{1/2} + C \tag{3.22}$$

where, k_p (mg g^{-1} $min^{-1/2}$) is the IPD rate constant. A plot of q_t versus $t^{1/2}$ yields C as intercept which estimates the thickness of the boundary layer around the adsorbent's surface. Larger the value of C, higher is the boundary layer effect.

3.9 Adsorption Isotherm

Adsorption isotherms are mathematical models that illustrate the distribution of adsorbate species between aqueous phase and adsorbent based on a combination of assumptions that are primarily related to the adsorbent's heterogeneity/homogeneity, the type of coverage and the potential of adsorbate species interaction.

3.9.1 Langmuir Isotherm

The Langmuir isotherm is based on the assumption of monolayer adsorption, that all adsorption sites are energetically similar, and that no adsorbate transmigrates across the surface [219], [222]. The Langmuir isotherm is defined as

$$q_e = \frac{q_o K_L C_e}{1 + K_L C_e} \tag{3.23}$$

Eq. 3.23 has been linearized in five different types of Langmuir isotherm as follows:

$$\text{Langmuir (Type – I)} \qquad \frac{C_e}{q_e} = \frac{1}{K_L q_{max}} + \frac{C_e}{q_{max}} \tag{3.24a}$$

$$\text{Langmuir (Type – II)} \qquad \frac{1}{q_e} = \frac{1}{q_{max}} + \frac{1}{K_L q_{max} C_e} \tag{3.24b}$$

$$\text{Langmuir (Type – III)} \qquad q_e = q_{max} - \frac{q_e}{K_L C_e} \tag{3.24c}$$

$$\text{Langmuir (Type – IV)} \qquad \frac{q_e}{C_e} = K_L q_{max} - K_L q_e \tag{3.24d}$$

$$\text{Langmuir (Type – V)} \qquad \frac{1}{C_e} = K_L q_{max} \frac{1}{q_e} - K_L \tag{3.24e}$$

where, K_L is Langmuir isotherm constant (L/g). Separation factor (R_L) was calculated to assess the favourability of adsorption.

$$R_L = \frac{1}{1 + K_L C_0} \tag{3.25}$$

The nature of adsorption process is favourable if ($0 < R_L < 1$), unfavourable ($R_L > 1$), linear ($R_L = 1$) and irreversible ($R_L = 0$).

3.9.2 Redlich-Peterson (R-P) Isotherm

The R-P isotherm combines the Langmuir and Freundlich isotherms. This is a hybrid model that deviates from the ideal monolayer adsorption law [222], [223]. It can be applied for both homogeneous and heterogeneous system [224], [225]. Eq. 3.26 represents R-P

isotherm.

$$q_e = \frac{K_R C_e}{1 + a_R C_e^g} \tag{3.26}$$

where, K_R (L/g) and a_R (L/mg) are R-P isotherm constant and g is an exponent.

3.9.3 Flory-Huggins (F-H) Isotherm

F-H isotherm depicts the extent to which the adsorbate covers the surface of the composite material [222], [223]. This isotherm model demonstrates the feasibility of adsorption and its spontaneity. The linear form of the isotherm is expressed in Eq. 3.27.

$$\ln\left(\frac{\theta}{C_0}\right) = \ln K_{FH} + n_{FH} \ln(1 - \theta) \tag{3.27}$$

where, θ is the degree of surface coverage, n_{FH} is the number of metal ions occupying adsorption sites and K_{FH} is F-H equilibrium constant (L/mol).

3.9.4 Temkin Isotherm

According to the Temkin equation, as equilibrium adsorption capacity increases, the heat of adsorption for all molecules in the layer drops linearly rather than logarithmically. The b_T factor is directly proportional to the affinity of material for the adsorbate [222], [223], [226]. The isotherm model is shown in Eq. 3.28.

$$q_e = \frac{RT}{b_T} ln\,(A_T C_e) \tag{3.28}$$

where, b_T is constant related to the heat of sorption (J/mol) and A_T is Temkin isotherm constant (L/g).

3.9.5 Toth Isotherm

When applied to porous materials, the Toth isotherm model is an empirical equation that was intended to improve the fit of the Langmuir isotherm type I model [222], [223]. It is

shown in Eq. 3.29.

$$q_e = \frac{q_{mT} C_e}{(a_T + C_e^z)^{1/z}} \tag{3.29}$$

where, q_{mT} is the uptake capacity of Toth isotherm (mg/g), a_T and z are Toth isotherm constants. The system heterogeneity is defined by Parameter 'z'. Higher is the deviation of z from unity, the more heterogeneous is the system. Parameter 'z' is temperature-independent, while a_T rises with the rise in temperature.

3.9.6 Hill Isotherm

This model considers that adsorption is supportive, with ligand binding occurring at a single place on the active site and affecting several binding sites on the same adsorbent.

$$\log \frac{q_e}{q_H - q_e} = n_H \, log\,(C_e) - log\,(K_D) \tag{3.30}$$

where, q_H is maximum uptake capacity of Hill isotherm (mg/g), K_D, and n_H are hill isotherm constants.There are three possibilities in this model: $n_H > 1$, positive binding; $n_H = 1$, non-cooperative or hyperbolic binding; $n_H < 1$, negative binding [223].

3.9.7 Sip Isotherm

It considers the Langmuir isotherm's monolayer adsorption capacity at high adsorbate concentrations [220], [223], [225]. The model has been shown in Eq. 3.31.

$$q_e = \frac{K_s C_e^{\beta s}}{1 - a_s C_e^{\beta s}} \tag{3.31}$$

where, K_s (L/g), a_s and βs are constants of sip isotherm.

3.9.8 Koble-Corrigan (K-C) Isotherm

The K-C isotherm is represented by a three-parameter equation that incorporates both the Langmuir and Freundlich isotherms [222], [225]. This model is usually only applicable

to heterogeneous sorbent surfaces when n_k >1 [223]. The model has been shown in Eq. 3.32.

$$q_e = \frac{AC_e^{n_k}}{1 + BC_e^{n_k}} \tag{3.32}$$

where, A, B and n_K are model constant

3.9.9 Fritz Schlunder-5 (FS-5) Isotherm

FS-5 isotherm model is valid for experimental data when α and β are ≤ 1. For this model, nonlinear methods of regression with higher complexities are required [223]. Eq. 3.33 represents FS-5 equation.

$$q_e = \frac{q_{mFS5} K_1 C_e^{\alpha_{FS}}}{1 + K_2 C_e^{\beta_{FS}}} \tag{3.33}$$

where, q_{mFS5} is maximum uptake capacity of FS-5 (mg/g), K_1 (mg/g), K_2 (mg/g), m_1 and m_2 are FS-5 isotherm constants.

3.9.10 Khan Isotherm

Khan isotherm is used for adsorption systems for single and multi-components [223]. The model has been shown in Eq. 3.34.

$$q_e = \frac{q_{max} b_k C_e}{(1 + b_k C_e)\, a_k} \tag{3.34}$$

where, a_K and b_K are Khan isotherm constants.

Eq. 3.34 reduces to the Langmuir isotherm when a_K - 1. This equation at the substantial C_e value reduces to Freundlich isotherm.

3.9.11 Radke-Prausnitz Isotherm

Radke and Prausnitz suggested that Langmuir isotherm can be slightly amended, introducing another factor which enhances the fitness of experimental information [222], [225].

Eq. 3.35 represents Radke-Prausnitz isotherm.

$$q_e = \frac{q_{mRP} K_{RP} C_e}{(1 + K_{RP} C_e)^{m_{RP}}} \tag{3.35}$$

where, q_{mRP} is maximum uptake capacity of Radke-Prausnitz isotherm (mg/g), K_{RP} and m_{RP} are Radke-Prausnitz isotherm constants.

3.9.12 Dubinin-Radushkevich (D-R) Isotherm

The D-R isotherm used to describe an adsorption system on a heterogeneous surface with a Gaussian energy distribution [222], [226]. This model is depicted in Eq. 3.36a. This model has been widely utilized to distinguish physical from chemical adsorption of metal ions using their mean free energy, E per adsorbate molecule, as computed by Eq. 3.36b [223]. Eq. 3.36c expresses the Polanyi potential of the D-R isotherm (ϵ).

$$ln\ q_e = ln\ q_m - \beta E^2 \tag{3.36a}$$

$$E = \frac{1}{\sqrt{2\beta}} \tag{3.36b}$$

$$\epsilon = RT \ln\left(1 + \frac{1}{C_e}\right) \tag{3.36c}$$

where, β is D-R isotherm constant (mol^2/kJ^2) and E is Energy of adsorption (J/mol).

3.9.13 Fowler-Guggenheim (F-G) Isotherm

F-G isotherm assumes lateral interaction of the adsorbing molecule. Eq.3.37 shows F-G isotherm.

$$\ln\left[\frac{C_e(1-\theta)}{\theta}\right] = -\ln K_{FG} + \frac{2w\theta}{RT} \tag{3.37}$$

where, w is interaction energy between adsorbed molecules (kJ/mol) and K_{FG} is F-G equilibrium constant (L/mg).

3.9.14 Elovich Isotherm

Elovich isotherm presumes that number of adsorption sites increases exponentially with adsorption, which represents multilayer adsorption [222], [223]. Eq.3.38 represents Elovich isotherm.

$$\frac{q_e}{q_m} = K_E C_e exp - \frac{q_e}{q_m} \tag{3.38}$$

where, K_E is Elovich isotherm constant (L/mg).

3.9.15 Freundlich Isotherm

Freundlich isotherm assumes the heterogeneous surface for adsorption to occur [219], [222]. Eq. 3.39a and Eq. 3.39b represents Freundlich isotherm.

$$\text{Non} - \text{linear form} \quad q_e = K_F C_e^{1/n} \tag{3.39a}$$

$$\text{Linear form} \quad log\ q_e = log\ K_F + \frac{1}{n}\ log\ C_e \tag{3.39b}$$

where, n and K_F (L/mg) are constant characteristics of the system. If n lies, between 1 to 10 adsorption is favorable.

3.9.16 Halsey Isotherm

Halsey isotherm has been used to study the multi-layer adsorption in relatively large distance from the surface [222], [223]. Halsey isotherm is shown in Eq. 3.40.

$$q_e = \frac{1}{n_H} lnK_H - \frac{1}{n_H} lnC_e \tag{3.40}$$

where,n_H and K_H (L/mg) are Halsey isotherm constants.

3.10 Thermodynamics

Thermodynamic adsorption parameters were investigated to determine process spontaneity, endothermic/ exothermic nature and randomness at solid-liquid interface. Eq. (3.41a-3.41c) were used to estimate the change in adsorption thermodynamic parameters.

$$\Delta G = -RT \ln K_D \tag{3.41a}$$

$$\Delta G = \Delta H - T\Delta S \tag{3.41b}$$

$$\ln K_D = \frac{\Delta H}{RT} + \frac{\Delta S}{R} \tag{3.41c}$$

where, K_D is equilibrium constant, R is universal gas constant (8.314 J/mol K), T is absolute temperature (K), ΔG is Gibbs free energy change (J/mol), ΔS (J/mol K) and ΔH (kJ/mol) are changes in entropy and enthalpy. The change in enthalpy represents an insight into the exothermic (if ΔH is negative) or endothermic (if ΔH is positive) nature of the process and also distinguishes between physio-sorption and chemisorption mode [227]. If adsorption is of physical type, the ΔH lies between -2.1 to -20.9 kJ.mol^{-1} and in chemisorption mode, ΔH ranges from -80 to -200 kJ.mol^{-1} [228].

3.11 Artificial Neural Network (ANN) Modeling

Empirical models framed using numerical estimate approaches such as ANN can be identified as an effective alternatives for predicting adsorption systems. ANNs were first created as a subset of the fundamental concept of artificial intelligence, which is to imitate the processes of the human brain and nervous system [229]. They are comprised of a set of mathematical correlations that serve to imitate the learning and memorizing processes. ANNs learn through example, which involves presenting a measured set of input variables and their associated output to ascertain the rules governing the relationship between the variables [229], [230]. In addition to this, the treatment of wastewater is complex and relies on various process parameters [231]. ANN is a smart network that can predict an

output pattern if a specific input data is known. Neural networks are primarily used for the study of large quantities of data sets. Neural network similarities can then be associated with new patterns, resulting in a forecast output pattern [232]. Back propagation is often used in engineering disciplines as a training algorithm. Because of its simple methodology and large training capacity, this method is often suggested. There are three layers in the back-propagation network algorithm: input, hidden, and output. The number of hidden layers in ANN can be increased depending on the type of problem [232]. ANN is an intelligent network capable of predicting an output function when a given input is identified. Neural networks are trained before implementing by simulating trustworthy experimental data sets [232]. The application of the empirical models, together with ANN, is one of the essential steps in prediction of output function [233]. Back-propagation is commonly used as a training algorithm in many fields, especially in engineering disciplines [234]. Modeling is a reliable and an effective mean to represent removal operations in engineering. Modeling and simulation of adsorption are well known techniques in environmental engineering because they can accurately predict the process [229]. Although percentage removal is a critical parameter for adsorption, it is not always available because of the time-consuming nature of data collection. ANN can be applied to adsorption since it is inspired by biological neuronal processing [229]. Batch adsorption studies were used to evaluate the adsorption of copper, nickel, and zinc ions onto novel adsorbents. ANN tool of MATLAB (version 9.1.0.26; license no.896539) was used for predictive modeling and comparing the experimental and predicted outcomes. Parameters such as pH, contact time, adsorbent dose, adsorbate concentration and temperature were fed as network inputs. In the present study, the technique of back propagation with the Levenberg-Marquardt (L-M) algorithm has been used. The percentage removal of Cu^{2+}, Ni^{2+} and Zn^{2+} ions were considered as output function. A set of parameters have been used for simulation. The network was trained until smaller number of epochs were attained [235]. After that, the data set was used to process the network simulation. The findings were correlated with experimental results.

3.12 Desorption Study

In order to remove the bonded metal ions adsorbed onto the adsorbents, the desorption test was carried out with distilled water and HCl as the stripping agent. The AAS was used to quantify the concentration of eluted metal in the filtrate after 0.1 g of dried metal laden adsorbent was mixed in 50 ml of 0.1 M HCl and agitated for 1 hour.

The percentage desorption was calculated by Eq. 3.42.

$$\%Desorption = \left[\frac{C_D \times V_D}{q_e \times m}\right] \times 100 \tag{3.42}$$

where, C_D (mg/L) indicates the concentration of metal ions in the desorbed solution, V_D (L) represents the volume of the desorbed solution, m (g) signifies the mass of the adsorbent utilized in the desorption studies and q_e (mg/g) refers the adsorption capacity of the adsorbent for metal ions.